Design and resonator-assisted characterization of high-performance lithium niobate waveguide crossings

Yikun Chen,[1] (iD) Ke Zhang,[1] Hanke Feng,[1] Wenzhao Sun,[2,3] and Cheng Wang[1,4,*] (iD)

[1]*Department of Electrical Engineering, City University of Hong Kong, Kowloon, Hong Kong, China*
[2]*Centre of Internet of Things, City University of Hong Kong Dongguan Research Institute, Dongguan, China*
[3]*Centre of Information and Communication Technology, City University of Hong Kong Shenzhen Research Institute, Shenzhen, China*
[4]*State Key Laboratory of Terahertz and Millimeter Waves, City University of Hong Kong, Kowloon, Hong Kong, China*
**cwang257@cityu.edu.hk*

Waveguide crossings are elementary passive components for signal routing in photonic integrated circuits. Here, we design and characterize two multimode interferometer (MMI)-based waveguide crossings to serve the various routing directions in the anisotropic x-cut thin-film lithium niobate (TFLN) platform. To address the large measurement uncertainties in traditional cut-back characterization methods, we propose and demonstrate a resonator-assisted approach that dramatically reduces the uncertainty of insertion loss measurement (< 0.021 dB) and the lower bound of crosstalk measurement (−60 dB) using only two devices. Based on this approach, we demonstrate and verify TFLN waveguide crossings with insertion losses of < 0.070 dB and crosstalk of < −50 dB along all three routing directions at 1550 nm. The low-loss and low-crosstalk waveguide crossings in this work, together with the simple and efficient characterization strategy, could provide important layout design flexibility for future large-scale classical and quantum TFLN photonic circuits. © 2023 Optica Publishing Group

Photonic integrated circuits (PICs) are promising components for next-generation communication and computing systems. However, while electronic very-large-scale integration (VLSI) utilizes complex three-dimensional routing structures, e.g., vertical vias and horizontal interconnections, to realize low-loss and compact multilayer signal routing, it is difficult to realize an optical counterpart using PICs, since optical vias suffer from high loss due to the sharp refractive index change at the vertical bends. Although multilayer waveguides could be implemented and linked via adiabatic tapers [1], the required fabrication processes are complicated and cost ineffective. In contrast, photonic interconnects could also cross over each other in a planar fashion via two-dimensional waveguide crossings, which are intriguing since they need only a single lithography step and are easy to implement. They have been applied to realize compact optical modulators [2], optical computing systems [3], quantum systems [4], etc. Although seemingly small for individual crossings, the insertion losses and cross talk of these

waveguide crossings are critical performance metrics, particularly for large-scale PICs, where vast amounts of waveguide crossings are adopted and their losses and crosstalk values cascade [3,4]. While some people make efforts to reduce the number of waveguide crossings by optimizing the routing algorithm [5], it is still a key research theme to improve the performance of waveguide crossings [6–11].

High-performance waveguide crossings have been achieved based on different principles, including inverse design [12], Gaussian beam synthesis [6], a sub-wavelength grating [7], multimode interference (MMI) [8–10], etc. MMI-based designs are the most widely adopted approach due to the ease of design, high fabrication robustness, and good performance. They have been demonstrated on silicon [8], polymer [9], and silicon nitride [10] platforms. However, investigations on thin-film lithium niobate (TFLN)—which is an emerging candidate for large-scale PICs owing to its low optical loss, large nonlinear coefficient, and commercial large-size wafer availability (up to 6 inches)—remain scarce. Benefiting from those properties, high-quality-factor (Q factor) micro-resonators [11], high-speed electro-optic modulators [13], and broadband frequency combs [14] have been realized. The development of high-performance TFLN waveguide crossings is indispensable for routing and intermediating between these devices in future large-scale PICs. On the other hand, traditional cut-back characterization of waveguide crossings often sees substantial measurement uncertainties, especially for small insertion losses, since the fiber-chip coupling losses ($\sim$ 5 dB/facet) [14] are usually much larger than the on-chip loss of an individual crossing (< 0.1 dB), and they vary substantially from device to device (they are commonly ± 0.4 dB). The difficulty in accurately determining the total optical loss is further exacerbated by the Fabry–Perot interference patterns resulting from reflections at the chip facets in edge-coupling setups. As a result, these measurements typically require a large number of cascaded crossings and averaging over many devices for a reasonably reliable estimation. Accurate measurements of small crosstalk values of these crossings are also highly non-trivial since the measurement lower bound (noise floor) could easily be affected by scattered light from other parts of the chip.
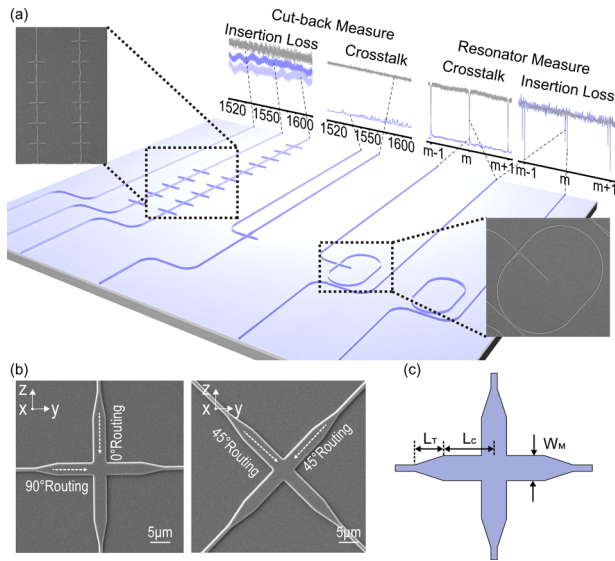
Fig. 1. (a) Schematic comparison of cut-back and resonator-assisted measurements of insertion loss and cross talk (insets: SEM images of fabricated devices). (b) Zoomed-in SEM images of the two crossing designs for routing along three crystal directions. (c) The geometric parameters that were swept to achieve the optimal designs.

Fig. 2. (a), (b) Simulated insertion loss as functions of the geometric parameters (a) W_M and L_C and (b) W_M and L_T along the 45° routing crystal direction. Stars denote the optimal parameters used in our experiment.

In this Letter, we address these issues by proposing a resonator-assisted measurement method where the waveguide crossing under test is embedded in a high-Q resonator. As a proof-of-concept, we design and fabricate low-loss MMI-based waveguide crossings in three routing crystal directions on an x-cut TFLN chip and precisely characterize the devices using our proposed method. Our experimental results show dramatically improved insertion loss measurement accuracy and a lowered crosstalk measurement floor compared with traditional cut-back approaches.

Figure 1(a) schematically illustrates the traditional cut-back method and our proposed resonator-assisted insertion loss and crosstalk characterization methods [the insets are scanning electron microscope (SEM) images of fabricated devices]. The traditional cut-back method compares the transmission spectra of multiple waveguides with different numbers of cascaded crossings to obtain the insertion loss from linear fitting [6,8–10,12], where the inaccurate estimation of fiber-chip coupling and the Fabry–Perot fringes resulting from the chip facets both contribute to the final measurement uncertainty. In contrast, our resonator-based method compares the Q factors of a reference micro-ring resonator and a crossing-embedded resonator to extract the difference in round-trip losses, which is not affected by uncertainties in fiber-chip coupling. This method is also not sensitive to fabrication variations between devices if the intrinsic cavity loss is much lower than the crossing loss. The effect of Fabry–Perot fringes can also be mitigated since we focus only on spectrally narrow resonance dips, especially for high-Q resonators. For crosstalk characterization, the traditional method that compares the transmission levels of the through and cross ports of a single crossing requires a large input power to reveal small crosstalk values and can easily be affected by scattered light from other parts of the chip, limiting the minimum crosstalk value we can measure. On the contrary, our resonator-enhanced approach can effectively bring the crosstalk signal up
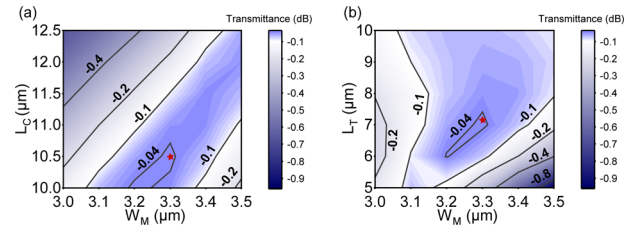
from the noise floor by magnifying the crosstalk power in the high-Q resonator.

To experimentally verify our proposed resonator-assisted measurement approaches, we first design two types of low-loss waveguide crossing to serve three popular routing directions in an anisotropic x-cut lithium niobate (LN) film, as illustrated in the SEM images in Fig. 1(b). Specifically, the left crossing device aligns along the y/z crystal directions, allowing z (0°)- and y (90°)-propagating signals to cross over each other with low cross talk, which requires an asymmetric design due to the different refractive indices along the y and z crystal directions. The right crossing device, on the other hand, routes along the 45° direction between y and z, and can be achieved using a symmetric design. We numerically simulate the MMI structure using full 3D finite-difference time-domain (FDTD) simulation (Ansys Lumerical). The anisotropic refractive index of LN is adopted to simulate the insertion loss and the cross talk along different routing crystal directions. The top width of the input/output waveguides, the rib waveguide thickness, the slanted sidewall angle of the rib waveguide, the slab thickness, and the oxide layer thickness are fixed to be 1 μm, 250 nm, 67°, 250 nm, and 2 μm, respectively, in accord with our typical fabricated TFLN device parameters. Geometric parameters, including the length of the taper L_T, the length of the MMI region L_C, and the top width of the MMI region W_M, are swept to achieve optimal designs with low loss and low cross talk for the fundamental transverse-electric (TE$_0$) mode in each design [Fig. 1(c)]. For an asymmetric design, these parameters are separately optimized for the 0° and 90° arms.

To serve as an example, Fig. 2 shows the simulated insertion losses for the symmetric crossing at 1550 nm as functions of L_C, L_T, and W_M. Stars denote the optimal insertion loss of 0.038 dB with geometric parameters of $W_M = 3.3$ μm, $L_C = 10.5$ μm, and $L_T = 7$ μm. The optimized asymmetric crossing has W_M, L_C, and L_T values of 3.4 μm, 12.5 μm, and 7 μm for the 90° arm and 3.2 μm, 10 μm, and 6 μm for the 0° arm. Devices are subsequently fabricated on a commercial x-cut LN-on-insulator wafer (NANOLN). A SiO$_2$ layer is first deposited. The pattern is then transferred to the SiO$_2$ layer using an ASML UV stepper lithography system (NFF, HKUST), which is followed by a reactive ion etching (RIE) process. Next, a second step of RIE transfers the pattern to the LN layer. Finally, the chips are cleaved for end-fire coupling [14]. Representative SEM images of the devices are shown in the insets of Fig. 1(a).
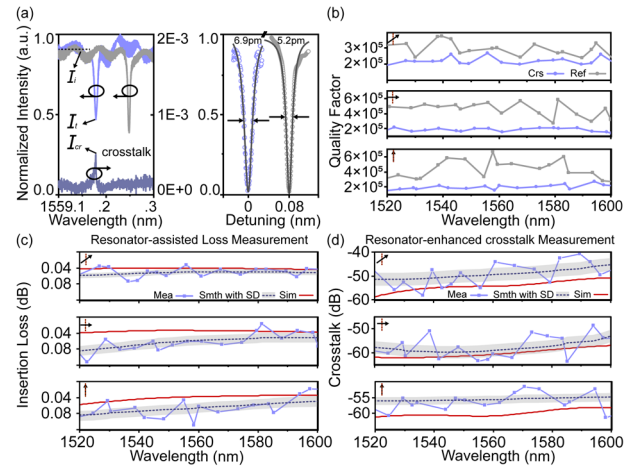
Next, we illustrate the limitations of traditional cut-back measurements by characterizing the insertion losses of the fabricated TFLN crossings. Figure 3(a) shows the normalized measured transmission spectra of the waveguides with different numbers of 45°-routing crossings, as measured using a
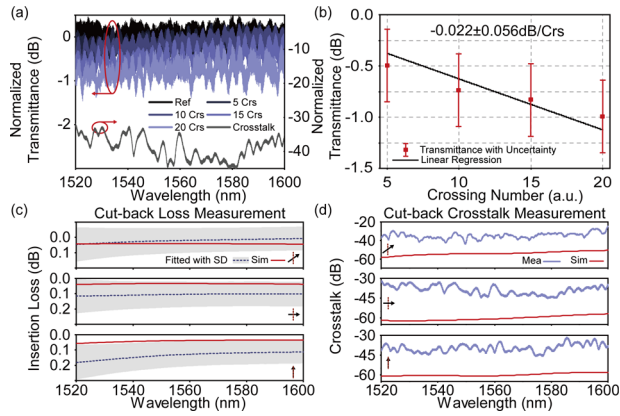
Fig. 3. Characterizations of TFLN crossings using traditional methods. (a) Measured transmission spectra for different numbers of cascaded 45° routing waveguide crossings (blue lines), and transmittance at the cross port of a single waveguide crossing (bottom gray line). (b) Linear regression of insertion loss at 1550 nm. (c) Fitted insertion loss spectra (blue dashed lines) with SD (shaded area) compared with simulation-predicted values (red) along three routing crystal directions (indicated by arrows). (d) Measured crosstalk (blue) spectra compared with simulation-predicted values (red) along three routing crystal directions.

Fig. 4. Resonator-assisted characterizations of TFLN crossings. (a) Left: example normalized transmission spectra of the through port of a crossing-embedded (bright blue) and a reference (gray) resonator, as well as the cross port of the crossing resonator (dark blue). Right: zoomed-in view and Lorentzian fit of the resonances. (b) Loaded Q factors of the reference resonator (gray) and the crossing-embedded resonator (blue) extracted at different wavelengths along three routing crystal directions (black arrows). (c), (d) Raw extracted (blue dots), smoothed (dashed blue), and simulated (red) values of (c) the insertion loss and (d) the cross talk at different wavelengths. Shaded areas show the SD of measurements.

broadband tunable laser (Santec TSL-550) followed by a polarization controller to launch the TE_0 mode and a lensed fiber for efficient coupling. The output light is collected by another lensed fiber and finally transmitted to a photodiode (PD). The measured transmittance decreases with an increasing number of crossings, and the trend can be fitted by a linear regression to estimate the insertion loss of a single crossing. Fabry–Perot interference fringes can be clearly observed in these spectra, and they add a measurement uncertainty (standard deviation, SD) of $\sigma_s = 0.510$ dB. Figure 3(b) shows the linear regression of this device with a fitted loss of 0.022 dB at 1550 nm and an uncertainty of 0.056 dB. The total measurement uncertainty is estimated as $\sigma_t = [(\sigma_s{}^2 + \sigma_c{}^2)/\Sigma_x]^{1/2}$, where $\sigma_c = 0.368$ dB is the SD (error bars) resulting from coupling and fabrication variation between different devices, and $\Sigma_x = \Sigma(x_i - \overline{X_i}) = 125$ is the summed deviation of the crossing number (x_i) of each cut-back waveguide from the mean number ($\overline{X_i}$). We calibrate σ_c by measuring the transmittances of four reference waveguides (without crossing) on the same chip and then using $\sigma_c = (\Sigma(T_i - \bar{T})^2/4)^{1/2}$, where T_i is the transmittance of each reference waveguide and $\bar{T}$ is the average transmittance. Notably, the estimated measurement uncertainty of 0.056 dB is substantially larger than the estimated loss (0.022 dB) itself, even though 5 separate devices with up to 20 crossings are tested, showing significant limitations when measuring small losses. By adopting the same method, we estimate the insertion losses of the two designs along three routing directions in Fig. 3(c) [the arrows in the insets indicate directions with respect to the optical axis (red dashed line)], where fitted insertion losses and measurement uncertainties are respectively given by blue dashed lines and the widths of shaded areas. The estimated insertion losses along 45°, 90°, and 0° at 1550 nm are, respectively, 0.022 ± 0.056 dB, 0.109 ± 0.055 dB, and 0.122 ± 0.064 dB, all showing large measurement uncertainties of > 0.050 dB.

Similar challenges are also present for small crosstalk measurements using traditional methods. The bottom gray curve

in Fig. 3(a) shows the crosstalk spectra. The measured crosstalk values (~ -40 dB) are significantly higher than our simulated results (~ -60 dB), which may result from scattered noise from defects on the chip and from facets. The measurement is also substantially limited by a relatively high noise floor of ~ -45 dB in our current measurement system, which could be estimated from the maximum laser output power of 13 dBm, the PD noise floor of ~ -50 dBm, the fiber-chip coupling loss of ~ 5 dB/facet [14], and a few dB of additional losses in other parts of the fiber link. Figure 3(d) summarizes the measured and simulated cross talk along the three routing directions, with all showing substantially higher (> 15 dB) measured crosstalk values than the simulated ones.

Finally, we characterize our designed waveguide crossings using our proposed resonator-assisted method, showing its significantly improved insertion loss measurement accuracy and lowered crosstalk measurement floor. Figure 4(a) shows example normalized intensity spectra of a crossing-embedded resonator along the 45° routing direction (bright blue line) and a reference resonator (gray line) fabricated side by side on the same TFLN chip. To optimize the loaded Q factor for a lower measurement uncertainty, the radius of the resonator is 80 μm to decrease the bending loss, while the coupling gap (700 nm) is designed for under-coupling to reduce the coupling loss. Lorentzian fitting [right panel of Fig. 4(a)] reveals a substantially lowered loaded Q factor of 226,000 for the crossing-embedded resonator compared with that of the reference resonator ($\sim 300,000$) due to excessive loss induced by the crossing. We can extract the round-trip amplitude transmission coefficient a of the resonators using the equation (see Supplement 1)

$$a = 1 - \frac{\pi n_g L}{2\lambda Q_L} - \sqrt{\frac{1}{T_t}} + \sqrt{\left(\frac{\pi n_g L}{2\lambda Q_L}\right)^2 - \frac{\pi n_g L}{\lambda Q_L} + \frac{1}{T_t}}, \quad \textbf{(1)}$$

where n_g and Q_L are the group index and loaded quality factor at the target wavelength λ, and L is the circumference of the resonator. $T_t = I_t/I_i$ is the on-resonance relative transmittance, where I_i and I_t are, respectively, the off-resonance and on-resonance light intensity. We can then estimate the insertion loss IL of the crossing by comparing the round-trip intensity transmittances of the crossing-embedded resonator ($a_c{}^2$) and the reference resonator ($a_r{}^2$) using the equation

$$IL = 10\log_{10}\frac{a_c{}^2}{a_r{}^2}. \tag{2}$$

Figure 4(b) shows the Lorentzian-fitted loaded Q factors for the three crossing directions. The fluctuations of the Q factors mainly come from the deformation of the Lorentzian shape under the influence of the background resonance fringes. Despite these fluctuations, we show much smaller insertion-loss measurement uncertainties [shaded areas in Fig. 4(c)] than the cut-back results in Fig. 3(c). The measurement uncertainty is calculated as $\sigma_t = (\sigma_s{}^2 + \sigma_c{}^2)^{1/2}$, where σ_s is the SD of the extracted insertion losses [blue dots in Fig. 4(c)], in this case < 0.018 dB, and σ_c is the SD due to fabrication variation between different resonators. We calibrate σ_c through statistical analysis of four reference resonators on the same chip, and we find it to be as small as ~0.009 dB (0.368 dB in the cut-back method). Importantly, none of the above analyses are influenced by fiber–chip coupling variations, leading to a small total insertion loss measurement uncertainty of ~ 0.02 dB, with only two devices needed. The measured insertion losses along the three directions around 1550 nm are, respectively, 0.051 ± 0.014 dB, 0.065 ± 0.013 dB, and 0.070 ± 0.021 dB, showing improved and lowered uncertainties (they are > 0.055 dB in the cut-back results) and good consistency with simulation results.

For crosstalk measurement, we monitor the output optical signals from the cross port of the crossing-embedded resonator, which show a resonance-enhanced crosstalk peak I_{cr} [dark blue line in Fig. 4(a)] at each resonant wavelength. We can estimate the cross talk of the crossing by using the equation

$$\text{Crosstalk} = 10\log_{10}\frac{T_c}{M}, \tag{3}$$

where $T_c = I_{cr}/I_i$ is the on-resonance relative crosstalk transmittance and M is the intensity amplification factor of the resonator, given by

$$M = \frac{1 - t^2}{(1 - a_c t)^2}. \tag{4}$$

Here, t is the amplitude transmission coefficient of the waveguide coupler, which can be estimated from the loaded Q factor by

$$t = 2 - a_c - \frac{\pi n_g L}{\lambda Q_c}. \tag{5}$$

Figure 4(d) illustrates the extracted crosstalk values of the three routing crystal directions, i.e., -50.1 ± 5.1 dB, -58.0 ± 5.1 dB, and -56.2 ± 2.8 dB, respectively, which are in much better agreement with our theoretical prediction. Thanks to the ~15 dB power amplification in our resonator, we bring down the lowest measured crosstalk values from ~ −45 dB in the traditional method to ~ −60 dB here, leading to much more accurate measurements of the real crosstalk values.

In conclusion, we have demonstrated two MMI-based waveguide crossings in x-cut TFLN that achieve insertion losses of < 0.070 dB and cross talk of < -50 dB at 1550 nm for all three routing directions. The ability to cross over waveguides with low losses and cross talk could provide layout-design flexibility for future large-scale TFLN PICs. Our designed waveguide crossings were characterized by a resonator-assisted method, which showed an improved insertion loss measurement accuracy of < 0.021 dB and a crosstalk measurement floor that was 15 dB lower compared with traditional cut-back methods. Both the insertion loss uncertainties and the minimum measurable cross talk can be further reduced by increasing the Q factor of the resonator through improved fabrication. Our proposed method provides an accurate and efficient solution to characterize waveguide crossings as well as other low-loss passive photonic elements, and is also applicable to other photonic platforms.

Disclosures. The authors declare no conflicts of interest.

Data availability. Data underlying the results presented in this paper are not publicly available at this time but may be obtained from the authors upon reasonable request.

Supplemental document. See Supplement 1 for supporting content.

REFERENCES

1. W. D. Sacher, Y. Huang, G. Q. Lo, and J. K. S. Poon, J. Lightwave Technol. **33**, 901 (2015).
2. G. Chen, K. Chen, J. Zhang, R. Gan, L. Qi, X. Fan, Z. Ruan, Z. Lin, J. Liu, and C. Lu, Opt. Express **30**, 25308 (2022).
3. J. M. Shainline, S. M. Buckley, R. P. Mirin, and S. W. Nam, Phys. Rev. Appl. **7**, 034013 (2017).
4. J. Wang, F. Sciarrino, A. Laing, and M. G. Thompson, Nat. Photonics **14**, 273 (2020).
5. T. Zhou and H. Jia, Opt. Commun. **413**, 230 (2018).
6. L. Han, X. K. Ruan, W. J. Tang, and T. Chu, Opt. Express **30**, 6738 (2022).
7. S. L. Wu, S. M. Mao, L. D. Zhou, L. Liu, Y. J. Chen, X. Mu, L. R. Cheng, Z. M. Chen, X. Tu, and H. Y. Fu, Opt. Express **28**, 27268 (2020).
8. M. Johnson, M. G. Thompson, and D. Sahin, Opt. Express **28**, 12498 (2020).
9. H. J. Zuo, S. L. Yu, T. Gu, and J. J. Hu, Opt. Express **27**, 11152 (2019).
10. H. M. Yang, P. F. Zheng, G. H. Hu, R. H. Zhang, B. F. Yun, and Y. P. Cui, Opt. Commun. **450**, 28 (2019).
11. R. Gao, N. Yao, J. Guan, L. Deng, J. Lin, M. Wang, L. Qiao, W. Fang, and Y. Cheng, Chin. Opt. Lett. **20**, 011902 (2022).
12. D. Yi, W. Zhou, Y. J. Zhang, and H. K. Tsang, Opt. Lett. **46**, 884 (2021).
13. C. Wang, M. Zhang, X. Chen, M. Bertrand, A. Shams-Ansari, S. Chandrasekhar, P. Winzer, and M. Lončar, Nature **562**, 101 (2018).
14. K. Zhang, W. Sun, Y. Chen, H. Feng, Y. Zhang, Z. Chen, and C. Wang, Commun. Phys. **6**, 17 (2023).